The $^{13}C(n,\alpha_0)^{10}Be$ cross section at 14.3 MeV and 17 MeV neutron energy

P. Kavrigin[1,a], F. Belloni[2], H. Frais-Koelbl[3], E. Griesmayer[1], A.J.M. Plompen[2], P. Schillebeeckx[2], and C. Weiss[1]

[1] CIVIDEC Instrumentation, Vienna, Austria
[2] EC-JRC Geel, Belgium
[3] Fachhochschule Wiener Neustadt, Austria

Abstract. At nuclear fusion reactors, CVD diamond detectors are considered an advantageous solution for neutron flux monitoring. For such applications the knowledge of the cross section of neutron-induced nuclear reactions on natural carbon are of high importance. Especially the (n,α_0) reactions, yielding the highest energy reaction products, are of relevance as they can be clearly distinguished in the spectrum. The $^{13}C(n,\alpha_0)^{10}Be$ cross section was measured relative to $^{12}C(n,\alpha_0)^{9}Be$ at the Van de Graaff facility of EC-JRC Geel, Belgium, at 14.3 MeV and 17.0 MeV neutron energies. The measurement was performed with an sCVD (single-crystal Chemical Vapor Deposition) diamond detector, where the detector material acted simultaneously as sample and as sensor. A novel data analysis technique, based on pulse-shape discrimination, allowed an efficient reduction of background events. The results of the measurement are presented and compared to previously published values for this cross-section.

1. Introduction

Diamond detectors based on CVD diamond can be efficiently used as neutron monitors due to the combination of such properties as: subnanosecond time response [1,2], high irradiation resistance [3,4], the possibility of discrimination of different particle interaction types [5,6]. The detection of fast neutrons with diamond detectors is achievable due to the nuclear reactions of neutrons with carbon nuclei [7]. Diamond detectors can be used for fast neutron flux monitoring and high-precision neutron spectroscopy [8].

An sCVD diamond detector was used for the cross section measurements at the Van de Graaff facility of the Joint Research Centre of the European Commission (EC-JRC) Geel. The measurements of the deposited energy spectra in the detector were performed with quasi-monoenergetic 14.3 MeV and 17.0 MeV neutron beams. A dedicated pulse-shape analysis method was used to efficiently separate background reactions, which allowed the selection of the nuclear reaction channels $^{12}C(n,\alpha_0)^{9}Be$ and $^{13}C(n,\alpha_0)^{10}Be$, and the derivation of the $^{13}C(n,\alpha_0)^{10}Be$ cross section relative to the one of $^{12}C(n,\alpha_0)^{9}Be$.

2. Experimental setup

In the experiment the 7 MV Van de Graaff accelerator installed at the EC-JRC was used as a neutron source with quasi-monoenergetic neutron beams with the mean neutron energies of 14.3 MeV and 17.0 MeV. The energy spectrum of the produced neutrons depends on the target type, the incident charged particle energy and the angle of the emitted neutron with respect to the incident charged particle beam. For the $^{13}C(n,\alpha_0)^{10}Be$ cross section measurements a 2 MeV deuteron beam impinging on a T/Ti target was used to produce neutrons via the $T(d,n)^4He$ reaction. The titanium layer of the target has 2157 $\mu g/cm^2$ areal density. The T/Ti atomic ratio was 1.0.

The equipment used in the experiment included:

- CIVIDEC [9] B1 Single-Crystal Diamond Detector (sCVD), with a thickness of 500 μm. The area of the detector electrodes is 4 mm by 4 mm. The detector was operated with an electric bias field of 1 V/μm. The detector was installed at 50 mm distance from the target.
- CIVIDEC C2 Broadband Amplifier with 2 GHz analogue bandwidth, 40 dB gain, and an equivalent input current noise of 0.4 μA_{rms}.
- LeCroy Waverunner 204-MXi digital oscilloscope with an analogue bandwidth of 1 GHz, sampling rate 10 GS/s and 8 bit resolution. The oscilloscope trigger level was set to +50 mV in the measurements, with 1000 pulses per recorded data buffer. The 50 Ω amplifier output was connected to the input of the oscilloscope using a 50 Ω cable.

The measurements were performed at two angles, $\theta_1 = 98^\circ$ and $\theta_2 = 45^\circ$ with respect to the direction of the deuteron beam. The mean neutron energy was 14.3 MeV at θ_1 angle and 17.0 MeV at θ_2 angle. The oscilloscope was used to record the amplified ionization current pulses from the detector. The area of the recorded pulses was used as a measure for the energy deposited within the detector. The experimental setup schematics is shown in Fig. 1.

The dead time between consecutive triggers in the continuous mode of the oscilloscope is not specified. Therefore, the absolute interaction rate in the detector

[a] e-mail: pavel.kavrigin@cividec.at

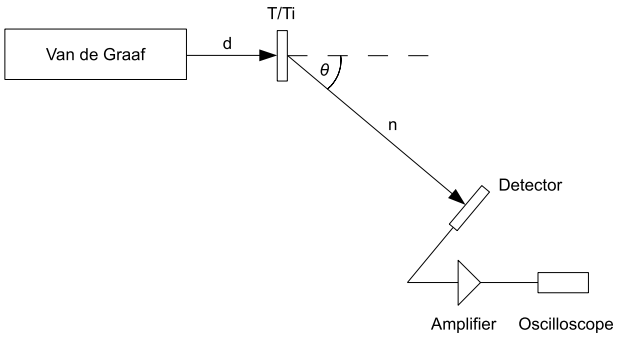

Figure 1. Schematic experimental setup.

could not be determined, and the relative cross section measurement was performed.

3. Data analysis

An sCVD diamond detector allows to derive the initial ionization profile in diamond from the detector current pulse. Therefore, it is possible to discriminate various types of incident particle interactions with the detector [5, 10].

In the case of *homogeneous ionization*, when the particle traverses the whole detector creating a uniform ionization along its linear track, the pulse shape is triangular. This type of ionization profile can be produced by high-energetic charged particles and by Compton electrons created by gammas.

In the case of a *point-like ionization*, the ionization current pulse is a superposition of rectangular pulses induced by the free charge carriers, i.e., electrons and holes. The resulting pulse shape is step-like for all interactions apart from the interactions in the ballistic center of the diamond. This type of ionization profile can be generated by charged particles produced in elastic and inelastic neutron reactions, and by alpha-particles and heavy ions which interact close to the electrode.

The *ballistic center* is defined as the location from which the drift times of electrons and holes are equal. The ballistic center is the only interaction location where a rectangular ionization current pulse is produced [10].

Pulse-shape analysis (PSA) of the ionization current pulses allows to determine the type of interaction. By selecting only the pulses corresponding to inelastic neutron reactions in the ballistic center, all other types of reactions occuring in any other locations can be separated. A detailed explanation of the analysis method is presented in [10].

In this measurement the following parameters were analyzed: (a) pulse amplitude, which corresponds to the initial ionization charge deposition; (b) pulse area, which corresponds to the total energy deposition; (c) base-width, which corresponds to the drift time of ionization charges. To select dedicated nuclear reaction channels three conditions were applied:

1. Amplitude condition, in order to select the interactions with an energy deposition higher than the ^{12}C(n,3α) break-up and to suppress all other interactions;
2. Drift time condition, used to select the interactions in the ballistic center, which have the minimum width;
3. Form factor condition, which is applied in order to select rectangular pulses which correspond to inelastic neutron reactions and to suppress other types of interactions that produce triangular and step-like pulse shapes. The form factor analysis is described in details in [10].

The deposited energy spectrum of neutrons in diamond includes the contributions of various nuclear reactions. A Geant4 simulation [11] was performed in order to obtain the deposited energy spectrum in the detector. The full geometry of the diamond detector was modelled. The incident neutron spectra for the simulation were determined using the TARGET code [12]. The neutron spectrum for the position at 98° was found to have a mean energy of 14.3 MeV and an energy spread of 182 keV FWHM. The neutron spectrum at 45° position was found to have a mean energy of 17.0 MeV and an energy spread of 370 keV FWHM. The simulated neutron spectra were used as the primary beam spectra in the Geant4 simulation.

The energy spectra of ^{12}C(n,α_0)^{9}Be and ^{13}C(n,α_0)^{10}Be simulated with Geant4 at 14.3 MeV and 17.0 MeV neutron energies were matched to the measured spectra, as shown in Figs. 2 and 3. The simulated spectra include a Gaussian broadening in order to account for the response function of the detector, and fit the simulated spectra to the measured spectra.

4. Measured spectra

The spectra of the deposited energy were measured. The calibration factor used to transform the area of the ionization current pulse into deposited energy was obtained from a comparison of the simulated and experimental spectra for the ^{12}C(n,α_0)^{9}Be reaction at 14.3 MeV neutron energy. From the experimental spectrum an area of 1085 pVs was derived for an average energy of 8.6 MeV in the simulated spectrum, which results in the energy conversion factor of 125.3 pVs/MeV. The detector system was calibrated using an unsealed ^{241}Am α-source. The corresponding conversion factor of 125.7 pVs/MeV matches the value derived using the simulation within 1%. The measurement with the α-source has also showed that the detector response is stable.

In Fig. 2 the measured spectra at 14.3 MeV neutron energy are shown. The total spectrum is shown in blue and the spectrum with the applied pulse-shape analysis is shown in red. The Geant4 simulation of ^{12}C(n,α_0)^{9}Be and ^{13}C(n,α_0)^{10}Be is shown in black.

In the total spectrum the elastic scattering process is dominant below 4.0 MeV. Events from the ^{12}C(n,3α) reaction result in an energy deposition between 5.0 MeV and 7.2 MeV. The ^{12}C(n,α_0)^{9}Be reaction has a peak with an average energy deposition of 8.6 MeV. The shoulder on the right side of the ^{12}C(n,α)^{9}Be peak results from high-energetic background events.

The three PSA criteria allowed to select the point-like interactions in the ballistic center with the initial ionization current above the ^{12}C(n,3α) edge. This way the nuclear reaction channels ^{12}C(n,α)^{9}Be and ^{13}C(n,α)^{10}Be were selected. All other interactions were rejected, in particular

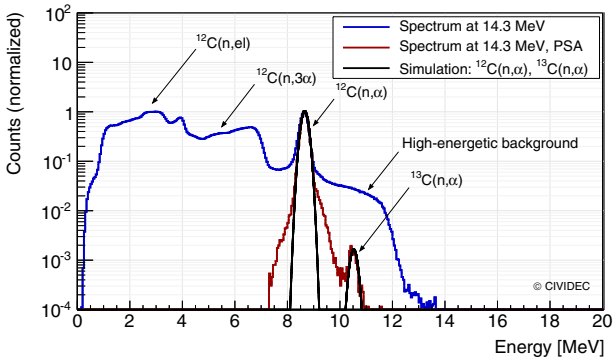

Figure 2. Deposited energy spectra at 14.3 MeV neutron energy: total spectrum (blue), spectrum with the applied pulse-shape analysis conditions (PSA, red), and spectra of ^{12}C(n,α_0)^{9}Be and ^{13}C(n,α_0)^{10}Be simulated with Geant4 (black).

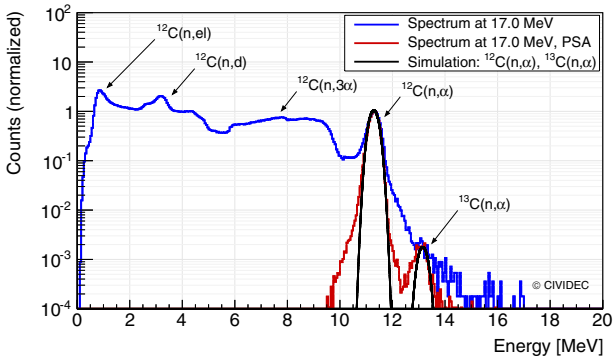

Figure 3. Deposited energy spectra at 17.0 MeV neutron energy: total spectrum (blue), spectrum with the applied pulse-shape analysis conditions (PSA, red), and spectra of ^{12}C(n,α_0)^{9}Be and ^{13}C(n,α_0)^{10}Be simulated with Geant4 (black).

the high-energetic background. The ^{13}C(n,α_0)^{10}Be peak is clearly visible at an average energy of 10.5 MeV. In the energy range from 10 MeV to 11 MeV, where the ^{13}C(n,α_0)^{10}Be peak is located, 99.2% of the pulses are rejected as high-energetic background.

In the simulated spectra the ^{12}C(n,α_0)^{9}Be peak has 312 keV FWHM and the ^{13}C(n,α_0)^{10}Be peak has 320 keV FWHM. The resulting energy resolution is influenced by the contribution of the detector system and by the neutron beam energy spread, as well as by the remnants of the high-energetic background at 14.3 MeV neutron energy.

In Fig. 3 the measured spectra at 17.0 MeV neutron energy are shown. The total spectrum is shown in blue and the spectrum with the applied pulse-shape analysis is shown in red. The Geant4 simulation of ^{12}C(n,α_0)^{9}Be and ^{13}C(n,α_0)^{10}Be is shown in black.

The total spectrum shows contributions from nuclear reactions, which are similar to the spectrum at 14.3 MeV. The ^{12}C(n,d) reaction peak is located at 3.3 MeV. The ^{12}C(n,3α) reaction results in an energy deposition between 6.0 MeV and 10.0 MeV. The ^{12}C(n,α_0)^{9}Be reaction has a peak with an average energy deposition of 11.3 MeV.

In the spectrum obtained using the PSA criteria the ^{13}C(n,α_0)^{10}Be peak is clearly visible at an average energy of 13.2 MeV. In the energy range from 12.5 MeV to 14 MeV where the ^{13}C(n,α)^{10}Be peak is located, 58.8% of the pulses are rejected as high-energetic background via the pulse-shape analysis.

Table 1. Measured ^{13}C(n,α_0)^{10}Be cross section.

Neutron energy(MeV)	σ_{12} (mb)	σ_{13}/σ_{12}	σ_{13} (mb)
14.3 ± 0.1	71.6	0.15	10.4 ± 1.1
17.0 ± 0.2	42.8	0.17	7.1 ± 0.7

In the simulated spectra the ^{12}C(n,α_0)^{9}Be peak has 418 keV FWHM and the ^{13}C(n,α_0)^{10}Be peak has 427 keV FWHM. The energy resolution is dominated by the neutron beam energy spread at 17.0 MeV neutron energy.

5. ^{13}C(n,α_0)^{10}Be cross section

The ratio of the ^{13}C(n,α_0)^{10}Be and ^{12}C(n,α_0)^{9}Be reaction was derived as:

$$\frac{\sigma_{13}}{\sigma_{12}} = \frac{I_{13}}{I_{12}} \cdot \frac{N_{12}}{N_{13}} \qquad (1)$$

where I_{12} and I_{13} are the net peak areas corresponding to the ^{12}C(n,α_0)^{9}Be and ^{13}C(n,α_0)^{10}Be reactions in the simulated spectra. N_{12} and N_{13} are fractions of ^{12}C and ^{13}C isotopes in diamond. The isotopic composition of carbon in sCVD diamond is equivalent to natural diamond, $N_{12} = (98.892 \pm 0.003)\%$ and $N_{13} = (1.108 \pm 0.003)\%$ of ^{13}C [13].

The evaluated total cross section ^{12}C(n,α)^{9}Be from CENDL-3.1 library [14] is used as σ_{12}, since the measurements of the partial cross section ^{12}C(n,α_0)^{9}Be reported in [15] clearly show that the ^{12}C(n,α_0) channel is dominant.

At the neutron energy of 14.3 MeV the ratio of the net peak areas is $I_{13}/I_{12} = (1.619 \pm 0.168) \cdot 10^{-3}$. The ratio of cross sections is $\sigma_{13}/\sigma_{12} = (0.15 \pm 0.01)$. Using the evaluated ^{12}C(n,α_0)^{9}Be cross section σ_{12}=71.6 mb at 14.3 MeV according to CENDL-3.1 library [14], the derived cross section of ^{13}C(n,α_0)^{10}Be is therefore $\sigma_{13} = (10.4 \pm 1.1)$ mb.

At the neutron energy of 17.0 MeV the ratio of the net peak areas is $I_{13}/I_{12} = (1.833 \pm 0.173) \cdot 10^{-3}$. The ratio of cross sections is $\sigma_{13}/\sigma_{12} = (0.17 \pm 0.01)$. Using the evaluated ^{12}C(n,α_0)^{9}Be cross section σ_{12} =42.8 mb at 17.0 MeV according to CENDL-3.1 library [14], the derived cross section of ^{13}C(n,α_0)^{10}Be is therefore $\sigma_{13} = (7.1 \pm 0.7)$ mb.

The uncertainty of the measured cross section includes:

- the uncertainty of the abundance of ^{13}C in diamond (N_{13}/N_{12}) which is 0.3% (from [13]);
- the I_{13}/I_{12} uncertainty which includes: (a) the statistical uncertainty dominated by the ^{13}C(n,α_0)^{10}Be statistics, with 5.9% for the measurement at 14.3 MeV with 291 counts, and 4.0% for the measurement at 17.0 MeV with 635 counts; (b) the uncertainty introduced by the analysis method dominated by the pulse width selection, estimated as a ratio of the 0.1 ns sampling period of the data acquisition system to the smallest recorded pulse baseline width of 1.2 ns, which is 8.3%;
- the energy resolution of the detector system which was 1.6% in the measurement at 14.3 MeV and 1.3% in the measurement at 17.0 MeV.

The total uncertainty is below 11% for both measurements. In Table 1 the measured ratios σ_{13}/σ_{12} and the corresponding cross sections σ_{13} of ^{13}C(n,α_0)^{10}Be are listed.

Previous measurement of ^{13}C(n,α_0)^{10}Be cross section was performed at the neutron energy range from 7.3 MeV

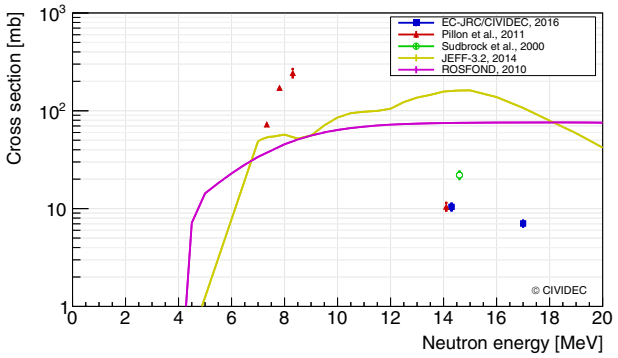

Figure 4. Measurements and evaluated data of ^{13}C(n,α_0)^{10}Be and ^{13}C(n,α)^{10}Be cross sections.

to 14.1 MeV [15]. The ^{13}C(n,α)^{10}Be total cross section was measured at 14.6 MeV [16]. The evaluated total cross section data for ^{13}C(n,α)^{10}Be is available in ROSFOND library (2010) and JEFF-3.2 library (2014). In Fig. 4 the measured ^{13}C(n,α_0)^{10}Be cross section values are shown, including the previously reported results for the partial and total cross sections. The measured cross section at 14.3 MeV is very close to the reported cross section at 14.1 MeV from [15]. The cross section at 17.0 MeV was measured for the first time. These measurements expand the available experimental dataset for this reaction.

6. Conclusions

The cross section of the ^{13}C(n,α_0)^{10}Be reaction was measured relative to the ^{12}C(n,α_0)^{9}Be reaction at 14.3 MeV and 17.0 MeV neutron energies. The nuclear reaction channels ^{12}C(n,α_0)^{9}Be and ^{13}C(n,α_0)^{10}Be were selected using a dedicated pulse-shape analysis method. The following results were obtained: $\sigma_{13}/\sigma_{12} = (0.15 \pm 0.01)$ at 14.3 MeV, $\sigma_{13}/\sigma_{12} = (0.17 \pm 0.01)$ at 17.0 MeV. Using the evaluated cross section of the ^{12}C(n,α)^{9}Be reaction from CENDL-3.1 [14], the ^{13}C(n,α_0)^{10}Be cross section was derived as $\sigma_{13} = (10.4 \pm 1.1)$ mb at 14.3 MeV, and $\sigma_{13} = (7.1 \pm 0.7)$ mb at 17.0 MeV.

The authors would like to thank EUFRAT for providing the facility and beam time, and the local team of the EC-JRC Van de Graaff accelerator for operating the neutron source.

References

[1] H. Frais-Kölbl, E. Griesmayer et al., IEEE Transactions on Nuclear Science **51**, 3833 (2004)
[2] H. Pernegger, S. Roe, P. Weilhammer, V. Eremin, H. Frais-Kölbl, E. Griesmayer et al., J. Appl. Phys. **97**, 073704 (2005)
[3] D. Husson et al., Nucl. Instrum. Methods Phys. Res. A **388**, 421 (1997)
[4] D. Meier et al., Nucl. Instrum. Methods Phys. Res. A **426**, 173 (1999)
[5] P. Kavrigin, P. Finocchiaro, E. Griesmayer, E. Jericha, A. Pappalardo, C. Weiss, Nucl. Instrum. Methods Phys. Res. A **795**, 88 (2015)
[6] C. Weiss, *A CVD diamond detector for (n,α) cross-section measurements*, PhD thesis (TU Wien, Vienna, 2014)
[7] M. Pillon, M. Angelone, A. Krasa, A.J.M. Plompen, P. Schillebeeckx, M.L. Sergi, Nucl. Instrum. Methods Phys. Res. A **640**, 185 (2011)
[8] C. Weiss, E. Griesmayer, C. Guerrero, S. Altstadt, J. Andrzejewski et al., Nucl. Instrum. Methods Phys. Res. A **732**, 190 (2013)
[9] `http://cividec.at`
[10] C. Weiss, H. Frais-Kölbl, E. Griesmayer, P. Kavrigin, Eur. Phys. J. A **52**, 269 (2016)
[11] Agostinelli, S. et al., Nucl. Instrum. Methods Phys. Res. A **506**, 250 (2003)
[12] D. Schlegel, *Target User's Manual* (PTB, Braunschweig, Germany), 2005
[13] J. Meija et al., Pure Appl. Chem. **88**, 293 (2016)
[14] Z.G. Ge et al., J. Kor. Phys. Soc. **59**, 1052 (2011)
[15] M. Pillon, M. Angelone, A. Krasa, A.J.M. Plompen, P. Schillebeeckx, M.L. Sergi, AIP Conf. Proc. **1412**, 121 (2011)
[16] F. Sudbrock et al., Radiochim. Acta **88**, 829 (2000)